Beat-note locking in dual-polarization lasers submitted to frequency-shifted optical feedback

Jérémie Thévenin,[1] Marc Vallet,[1,*] Marc Brunel,[1] Hervé Gilles,[2] and Sylvain Girard[2]

[1]*Institut de Physique de Rennes, UMR Université de Rennes 1, CNRS, Campus de Beaulieu, F-35042 Rennes Cedex, France*

[2]*Centre de Recherche sur les Ions, les Matériaux et la Photonique, UMR ENSICAEN–Université de Caen–CNRS–CEA, 6 Boulevard Maréchal Juin, F-14050 Caen Cedex, France*

**Corresponding author: marc.vallet@univ-rennes1.fr*

Received December 22, 2010; revised March 10, 2011; accepted March 10, 2011; posted March 11, 2011 (Doc. ID 139995); published April 15, 2011

We derive a delay-differential equation model that describes continuous-wave (cw) or passively *Q*-switched (PQS) two-frequency solid-state lasers submitted to frequency-shifted feedback (FSF). The study focuses on the locking of the beat note between the two free-running laser frequencies to a reference external frequency. The locking domain is obtained analytically in the cw regime. The PQS regime is treated by adding a saturable absorber population in the model equations. In this case, numerical simulations permit us to evaluate a locking range that is smaller than in the cw case. We find good agreement between the theoretical predictions and experiments carried out with a cw diode-pumped dual-polarization Nd:YAG laser as well as with previously published experimental results obtained with cw Er:Yb:glass [Opt. Lett. **32**, 1099 (2007)] and PQS Nd:YAG [Opt. Lett. **33**, 2524 (2008)] lasers. Applications of the FSF locking technique include the lidar–radar technique, for which a highly coherent beat note is required.

OCIS codes: 140.3430, 140.3520, 140.3580.

1. INTRODUCTION

Lasers exposed to optical feedback are the subject of numerous theoretical and experimental studies, whether for practical reasons, such as the search for better laser stability, or for academic reasons when the laser shows a generic dynamical behavior. When the optical feedback loop includes a frequency shifter, typically an acousto-optic Bragg cell, various dynamics have been reported—especially in diode-pumped solid-state lasers. A first class of frequency-shifted feedback (FSF) can be identified as destabilizing. It is well known that solid-state laser dynamics is governed by the relaxation oscillation frequency f_R. Hence, when the feedback light is shifted in frequency by f close to f_R, the laser is strongly destabilized [1]. Otsuka showed that Doppler velocimetry is a useful application of this effect in single-frequency microchip lasers [2], while Lacot *et al.* further demonstrated an imaging technique based on the same effect [3]. In addition, when the laser operates in a two-frequency regime, the sensitivity of the laser to the FSF is even stronger, as proved by Nerin *et al.* [4] and Kervevan *et al.* [5]. Another kind of FSF scheme can also lead to destabilization: if one imposes inside the laser cavity a frequency shift that is far greater than f_R, the laser exhibits a nonconventional frequency spectrum, once known as a "modeless" spectrum. This was first observed in dye lasers by Kowalski *et al.* [6] and recently understood as a broadband cyclostationary thermal spectrum [7]. In the case of solid-state lasers, intracavity FSF can also lead to pulsed regimes [8]. The second class of FSF can be identified as stabilizing. Indeed, considering a dual-polarization two-frequency laser characterized by its beat frequency $f_b \gg f_R$, Kervevan *et al.* have shown that a feedback with a frequency shift f in the vicinity of f_b can lock this beat pulsation [9]. The continuous-wave (cw) laser beat note can be efficiently stabilized against the usual technical drifts. It was then demonstrated using the same principle that a passively *Q*-switched (PQS) two-frequency laser could also be stabilized. This offered a means to induce coherence in the beat note from pulse to pulse [10]. These studies, however, lacked theoretical support. No model of two-frequency lasers submitted to a FSF has been developed yet.

The aim of this article is hence to provide a theoretical model describing FSF two-frequency lasers, both in the cw and PQS regimes. We propose to derive a delay-differential equation system reminiscent of the Lang–Kobayashi model [11]. The model is compared with the experimental results obtained in [9,10]. In addition, we perform here experiments with a cw diode-pumped Nd^{3+}:YAG laser containing a birefringent element for dual-polarization two-frequency operation. The remainder of the article is organized as follows. In Section 2, we introduce the laser rate equations, taking into account the FSF term. An analytical expression of the locking range is found in the cw case. In Section 3, the experimental results are reported and compared with simulation results. Finally, conclusions are given in Section 4.

2. THEORETICAL MODEL

Ordinary single-mode cw solid-state lasers are well described by two coupled rate equations for the population inversion in the active medium and the photon number in the laser resonator [12]. In the presence of a time-delayed reinjected field, it was shown in [1] that the Lang–Kobayashi equations first derived for semiconductor lasers describe correctly the operation of rare-earth-doped lasers. Moreover, these equations can be extended to the case of a FSF [3]. However, the case of a dual-polarization two-frequency laser has never been analyzed in this framework. This will be our first aim of the following analysis. Furthermore, when a saturable absorber is inserted

inside the cavity, a third equation governing the evolution of the population inversion in the absorber has to be added to predict the pulsed operation [12]. In the vectorial anisotropic case, the absorber is well described using a set of three equations for the absorber inversion populations [13]. Our second aim in the analysis is hence to start from the PQS laser equations and introduce the time-delayed term in order to study the locking effects in the pulsed case. After a short description of the setup in Subsection 2.A, the two cases of cw and PQS lasers will be considered separately in Subsections 2.B and 2.C.

A. Description of the System

Let us consider the laser cavity of Fig. 1, whose propagation axis is z. It is closed with mirrors M_1 and M_2 and contains an isotropic active medium AM and a pair of quarter-wave plates $QWP_{1,2}$. This linear phase anisotropy $\Delta\varphi_{x-y}$ leads to cavity eigenfrequencies ν_x and ν_y associated to the x and y eigenpolarizations [14,15]. It may also contain an optional etalon (not shown) that enforces single-longitudinal mode operation. For the PQS operation, a saturable absorber, SA, is inserted inside the cavity. The laser beam contains two orthogonal linear field components E_x and E_y. The output beam propagates through an acousto-optic Bragg cell, AO, driven continuously by an RF signal with a frequency f_{AO}. Mirror M_3 is aligned in order to feed the first diffraction order back to the laser, as shown in Fig. 1. As a result of this particular feedback scheme, the beam coming back to the laser is frequency shifted by $2f_{AO}$. Note that a polarization rotator, PR, for instance a Faraday rotator or a quarter-wave plate, inserted between AO and M_3 permits us to rotate the polarization by 90°. In the model, we study the laser fields E_x and E_y considering a feedback in which the electric field E_x is frequency shifted and polarization rotated along the y axis before being reinjected.

B. Model for the Continuous-Wave Regime

Starting from the two-mode rate equations [16], here with the electric fields written in complex form, and neglecting the spatial hole-burning effects, the population inversions of the laser eigenstates are written as

$$\dot{n}_{x,y} = \gamma_{//}P_{x,y} - [\gamma_{//} + \zeta(|E_{x,y}|^2 + \beta|E_{y,x}|^2)]n_{x,y} + \tilde{n}_{x,y}, \quad (1)$$

where $\gamma_{//}$ is the decay time of the population inversion in the gain medium; $P_{x,y}$ are the pumping rates of the x and y eigenstates, respectively; β is a coupling constant accounting for cross-saturation in the gain medium; and $\tilde{n}_{x,y}$ are Langevin noise terms accounting for spontaneous emission. The rate equations for the fields, taking the feedback term along the y polarization into account, are written as

$$\dot{E}_x = \{i2\pi\nu_x + [-\Gamma_x + \kappa(n_x + \beta n_y)]/2\}E_x + \tilde{E}_x, \quad (2)$$

$$\dot{E}_y = \{i2\pi\nu_y + [-\Gamma_y + \kappa(n_y + \beta n_x)]/2\}E_y + \tilde{E}_y + \gamma_e E_x(t-\tau)e^{i(4\pi f_{AO}t+\psi)}. \quad (3)$$

In these equations, $\Gamma_{x,y}$ are the laser cavity decay rates along the x and y directions, given by $\Gamma_{x,y} = -c/2L \times \ln[R_1R_2(1-\delta_{x,y})^2]$, where R_1 and R_2 are the intensity reflection coefficients of mirrors M_1 and M_2, respectively, and δ_x and δ_y are the single-pass loss coefficients experienced by x and y eigenstates through propagation inside the cavity. κ and ζ are the constant field–atom coupling coefficients. Following [3], the last term on the right-hand side of Eq. (3) is the delayed term standing for the feedback field. It contains the frequency shift $2f_{AO}$, and τ and ψ, which are the external round-trip time and phase shift in the feedback cavity (between M_2 and M_3). γ_e is the feedback strength parameter that can be written $\gamma_e = g\Gamma_y\sqrt{R_3}$, where R_3 is the intensity reflection coefficient of the feedback cavity, including the reflectivity of mirror M_3, the overall diffraction efficiency (two-pass) of the AO cell, and the transmissions of the various optical elements. g is a constant characterizing the spatial overlap between the feedback beam and the intracavity laser beam [3]. Equations (1)–(3) can be simplified by considering $E_x = E_x e^{i2\pi\nu_x t} = |E_x|e^{i(2\pi\nu_x t+\phi_x)}$ and $E_y = E_y e^{i2\pi(\nu_x+2f_{AO})t} = |E_y|e^{i2\pi(\nu_x+2f_{AO}t+\phi_y)}$. In addition, we take $\kappa = \varsigma = 1$, $\delta_x = \delta_y$ yielding $\Gamma_x = \Gamma_y \equiv \Gamma$, and $P_x = P_y$. We define the detuning $\Delta\nu = \nu_y - \nu_x - 2f_{AO}$. We write η the excitation ratio above threshold and $n_0 = \Gamma/(1+\beta)$ the population inversion at threshold. We assume a constant feedback phase, and we take $-2\pi\nu_x\tau + \psi = 0$. Using all these simplifications, the laser two-mode equations become

$$\dot{n}_{x,y} = \gamma_{//}\eta n_0 - (\gamma_{//} + |E_{x,y}|^2 + \beta|E_{y,x}|^2)n_{x,y} + \tilde{n}_{x,y}, \quad (4)$$

$$\dot{E}_x = (-\Gamma + n_x + \beta n_y)E_x/2 + \tilde{E}_x, \quad (5)$$

$$\dot{E}_y = (-\Gamma + n_y + \beta n_x)E_y/2 + i2\pi\Delta\nu E_y + \tilde{E}_y + \gamma_e E_x(t-\tau). \quad (6)$$

In the following, we use Eqs. (4)–(6) to derive analytically the locking range that will be compared in Section 3 to the experimental results. Finally, as in [3], the population noise terms are $\tilde{n}_{x,y} = 0$, and the electric field Langevin noise terms are assumed to be proportional to the optical gain and can be written as $\tilde{E}_{x,y} = (n_{x,y} + \beta n_{y,x})\varepsilon$, where ε is a constant.

We now focus on the locking range. Deriving the evolution of the phases from Eqs. (5) and (6), one gets the following Adler equation:

$$\dot{\phi}_y = 2\pi\Delta\nu - \gamma_e\left|\frac{E_x(t-\tau)}{E_y(t)}\right|\sin[\phi_y(t) - \phi_x(t-\tau)]. \quad (7)$$

This demonstrates that the feedback term may induce a phase-locking effect. The locking range can be evaluated by stating that the stationary state corresponds to constant

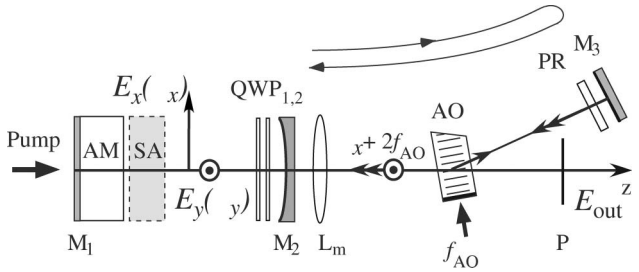

Fig. 1. Schematic of the experimental setup. Two-frequency laser: M_1 and M_2, cavity mirrors; AM, active medium; $QWP_{1,2}$, quarter-wave plates; $E_{x,y}$, cross-polarized intracavity fields; $\nu_{x,y}$, eigenfrequencies; SA, saturable absorber (pulsed regime only). Reinjection arm: AO, acousto-optic frequency shifter driven at frequency f_{AO}; PR, polarization rotator; M_3, mirror; L_m: matching lens; τ, feedback round-trip time. Output: P, polarizer, E_{out}, output field.

phases $\phi_{x,y}$ and intensities $|E_{x,y}|^2$. We also consider that, at equal losses, the feedback term leads to an intensity associated to the y eigenstate slightly larger than the one associated to the x eigenstate, i.e., $|E_y|^2 \geq |E_x|^2$. The locking range is then straightforwardly obtained from Eq. (7):

$$-\gamma_e/2\pi \leq \Delta\nu \leq \gamma_e/2\pi. \tag{8}$$

The dependence of the locking range on the feedback strength will be analyzed experimentally and numerically in Section 3. Before doing so, we extend the model to the PQS regime.

C. Passively *Q*-Switched Regime

We assume that the saturable absorber, which provides the cavity Q-switching mechanism, allows the simultaneous emission of x- and y-polarized pulses. It was shown, for example, that an intracavity absorber consisting of a [001]-cut Cr^{4+}:YAG plate, with the [001] crystallographic axis aligned along the cavity optical axis, fulfills this condition if the intracavity phase anisotropy axes are oriented at 45° with respect to the Cr^{4+}:YAG axes [13]. Under this condition, we derive the modified rate equations. First, we note that the population inversion is left unchanged. Equation (4) will thus be used for simulations of the PQS regime. Second, the electric field equations become:

$$\dot{E}_x = (-\Gamma + n_x + \beta n_y - a_x)E_x/2 + \tilde{E}_x, \tag{9}$$

$$\dot{E}_y = (-\Gamma + n_y + \beta n_x - a_y)E_y/2 + i2\pi\Delta\nu E_y + \tilde{E}_y + \gamma_e E_x(t-\tau). \tag{10}$$

Equations (9) and (10) differ from Eqs. (5) and (6) by the saturable absorption terms. $a_{x,y}$ are the saturable loss coefficients along the x and y axes. When the [100] axis is set at 45° with respect to the x direction, they are equal to the mean of the saturable loss coefficients associated to the [100] and [010] crystallographic axes. Third, writing $a_x = a_y = a$, the time evolution of the absorber is governed by

$$\dot{a} = \gamma_a a_0 - [\gamma_a + \mu_0(1 + C_a)(|E_x|^2 + |E_y|^2)/2]a, \tag{11}$$

where $a_0 = -c/L \times \ln(T_a)$ is the unsaturated absorption coefficient. T_a is the single-pass intensity absorption. γ_a is the decay rate of the excited state of the absorbing transition. The coupling coefficient μ_0 is written as $\mu_0 = \sigma_a/\sigma_g$, where σ_a (σ_g) is the absorption (stimulated emission) cross section of the absorbing (laser) transition in the absorber (gain medium) [13]. C_a accounts for the cross-saturation in the absorber. Finally, the population inversion at threshold then becomes $n_0 = (\Gamma + a_0)/(1 + \beta)$. In contrast with the cw case, here there is no simple analytical expression for a locking range. We will see, however, that a locking phenomenon still occurs. Equations (4) and (9)–(11) will be numerically integrated in Section 3 to simulate the behavior of the dual-polarization PQS laser submitted to the FSF. For the sake of clarity regarding the interpretation of the experimental observations, we now discuss briefly the differences between unlocked and locked pulsed beat notes [17] following Fig. 2. Let us consider the intensity of a periodic pulse train at a repetition rate f_{rep} containing a beat note at frequency $f_b = \nu_y - \nu_x$, as depicted schematically in Fig. 2(a). If the coherence time of the beat-note phase $\phi = \phi_y - \phi_x$ is shorter than f_{rep}^{-1} the beat-note coherence is limited to the duration of one pulse only. Then the beat-note spectrum exhibits a smooth shape as schematized in the left plot of Fig. 2(b). Conversely, if due to the locking mechanism, ϕ is constant over an infinite time, then the beat-note spectrum is an f_{rep}-periodic spectral comb around f_b, as schematized in the right plot of Fig. 2(b). This second case corresponds to a perfectly coherent beat note from pulse to pulse, locked to the local oscillator, as indicated in Fig. 2(a). This simple Fourier analysis shows that an experimental spectrum of the beat note permits us to check whether the FSF turns the pulsed beat note from incoherent (or unlocked, with a smooth spectrum) to phase locked (exhibiting an f_{rep}-periodic spectrum).

3. EXPERIMENTAL RESULTS AND SIMULATIONS

The two-frequency laser used in the experiment is schematized in Fig. 1. The cavity of length $L = 75$ mm is closed by a high-reflection plane mirror M_1, which is coated on the 5 mm long Nd:YAG gain crystal AM, and concave mirror M_2, whose radius of curvature is 100 mm and whose intensity transmission is 1% at the lasing wavelength $\lambda = 1064$ nm. The Nd:YAG is pumped by a laser diode at 808 nm. A 1 mm thick silica etalon (not shown) ensures single-longitudinal-mode oscillation. Two orthogonally polarized eigenstates are obtained by introducing a pair of antireflection-coated quarter-wave plates (QWPs) inside the cavity [14]. Here the orientations of $QWP_{1,2}$ are chosen to obtain a beat frequency at around $f_b = 180$ MHz. The typical power emitted by the two-frequency laser is 10 mW when pumped with 500 mW.

The feedback scheme is schematized in the right-hand part of Fig. 1. The laser output waves at frequencies ν_x and ν_y are frequency shifted by an acousto-optic Bragg cell AO driven by a radio frequency (RF) generator. The RF power is variable, but power of 24 dBm at the acoustic frequency $f_{\mathrm{AO}} = 90$ MHz is typical. The upconverted waves in the first diffraction order

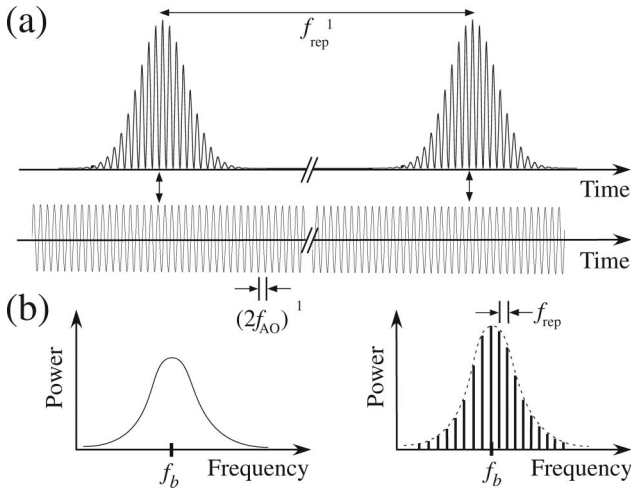

Fig. 2. (a) Schematic of a pulse train (repetition rate f_{rep}) carrying a beat note locked to $2f_{\mathrm{AO}}$. (b) Schematic of the output RF spectra corresponding to (left) an incoherent beat note at f_b delivered by a free-running laser, or to (right) a fully coherent beat note locked to $f_b = 2f_{\mathrm{AO}}$.

are fed back to the laser after one round trip in a polarization rotating setup (see PR in Fig. 1). It includes an antireflection-coated quarter-wave plate whose neutral axes are rotated at 45° with respect to the x and y directions, and a high-reflection mirror M_3. The feedback cavity length is 75 cm, corresponding to a round-trip time of 5 ns. A lens L_m is inserted for matching the feedback mode to the laser mode. Following the wave at the initial frequency of ν_x (and supposing $\nu_y > \nu_x$), we find that, after one complete round trip inside the feedback cavity, this wave seeds the laser with a frequency of $\nu_x + 2f_{AO}$ and a polarization parallel to the y eigenstate. When the laser beat frequency approaches the doubled driving frequency of the AO ($|\Delta\nu| \leq \gamma_e$), phase locking is expected to occur. Note that, in contrast to [9], the other wave at frequency ν_y is also fed back to the laser, but with an upconverted frequency away from the laser eigenfrequencies. It does not affect the laser behavior. Monitoring the optical spectrum with a Fabry–Perot analyzer, we verified that it does not contain any component at $\nu_y - \nu_x + 2f_{AO}$ and that the laser oscillates in a pure two-frequency regime at all times. The beam in diffraction order 0 provides the useful output signal that is sent through a polarizer oriented at 45° with respect to the laser eigenpolarization directions (x and y). This output field (labeled E_{out}) is detected thanks to a 2 GHz bandwidth photodiode connected to either an oscilloscope or a spectrum analyzer.

A. Continuous-Wave Two-Frequency Laser

In free-running operation, i.e., without feedback, the laser beat note fluctuates due to technical noises with a typical rate of 10 kHz/s around the value of 180 MHz. When feedback is applied, different behaviors are observed depending on the values of the detuning $\Delta\nu$ and of the feedback strength γ_e. Both parameters are driven by the AO cell (f_{AO} and diffraction efficiency). Note that, in order to take into account possible polarization-dependent diffraction efficiency, we report the mean diffraction efficiency over one round trip inside the AO cell. First, we choose $f_{AO} = 89.5$ MHz and a RF power of 24 dBm, which leads to a diffraction efficiency of 56%. These values correspond to a detuning $\Delta\nu$ of about 1 MHz and a feedback reflectivity R_3 of about 0.2. Figure 3(a) shows the electrical spectrum of the output beam. One can see two peaks: the peak on the right-hand side corresponds to the beat note between the two eigenstates E_x and E_y, and the peak on the left-hand side corresponds to the beat note between one eigenstate and the frequency-shifted field after one round trip inside the feedback cavity, hence at frequency $2f_{AO}$. In this case, the detuning is obviously outside the locking range. When the RF frequency is swept by a few hundred kilohertz more, there is a sudden jump of the beat note to the reference frequency $2f_{AO}$. Locking occurs, and the resulting spectrum contains a single beat line at frequency $2f_{AO}$, as shown in Fig. 3(b). $2f_{AO}$ can then be tuned by 1.6 MHz, and the beat note stays locked. In the locking range, a close inspection of the peak reveals that the beat note replicates perfectly the RF synthesizer line. Indeed, as one can see in the inset of Fig. 3(b), the peak has an instrument-limited full-width at half-maximum (FWHM) of 1 Hz.

The locking range is governed by Eq. (8). The only experimental parameter that we can actuate in a reproducible way is the diffraction efficiency. Figure 4 reports the measured locking range when the RF power of the AO cell is varied from +15 to +30 dBm. It corresponds to diffraction efficiencies ranging from 10% to 90%. The evolution of the locking range is linear and reaches almost 4 MHz. This can be compared to the theoretical full locking range given by Eq. (8). The experimental value of R_3 is simply evaluated by the product of the diffraction efficiency times the different transmissions of the optical elements inside the feedback cavity. The cavity loss rate is evaluated to be $\Gamma = 4 \times 10^7\ s^{-1}$, assuming a single-pass loss rate of $\delta = 0.006$. The theoretical expression of the full locking range $\gamma_e/\pi = g\Gamma\sqrt{R_3}/\pi$ fits the experimental results if $g = 0.3$. This is a reasonable estimate of the overlapping factor. By integrating Eqs. (4)–(6) with the standard MATLAB routine dde23, we verified numerically that the locking range fits the analytical expression of Eq. (8). The agreement between the theoretical predictions and the experimental results tends to justify the approximations used, in particular the fact that a single round-trip in the feedback cavity has to be taken into account. Finally, Eq. (8) is also compared to the experimental locking range obtained with the two-frequency Er:Yb:glass laser described in [8]. The measured 300 kHz locking range fits the theoretical value if $g \cong 0.05$. Again, this is a fair estimate of the experimental overlapping factor.

B. Passively *Q* Switched Two-Frequency Laser

For completeness, we recall briefly the results described in [9]. In order to operate the laser in a pulsed passively Q-switched regime, a [100]-cut Cr:YAG saturable absorber crystal SA, whose unsaturated intensity transmission coefficient is $T_a = 0.90$, is inserted between the AM and the QWPs (see Fig. 1). The orientations of the neutral axes of crystals SA and QWPs are chosen to obtain the simultaneous oscillation of the two orthogonal, linearly polarized, eigenstates with a tunable frequency difference up to $c/4L$ [13]. The measured characteristics of the output laser pulses are typical of Nd:YAG lasers passively Q switched by Cr:YAG. The laser emits a stable pulse train with a repetition rate of $f_{rep} = 10$ kHz at a pump power of $P = 0.7$ W. The pulse energy and duration are 3 μJ and $\tau = 45$ ns (FWHM), respectively. Measurement of the pulsed output versus time yields the result depicted in Fig. 5(a). The beat note between the two laser eigenfrequencies, here phase locked at $2f_{AO} = 185$ MHz, appears inside the pulse envelope. Note that (i) the orientation of P is experimentally adjusted in order to get a beat-note maximal modulation depth and (ii) outside the locking range, the output pulses are identical to the one reported in Fig. 5(a).

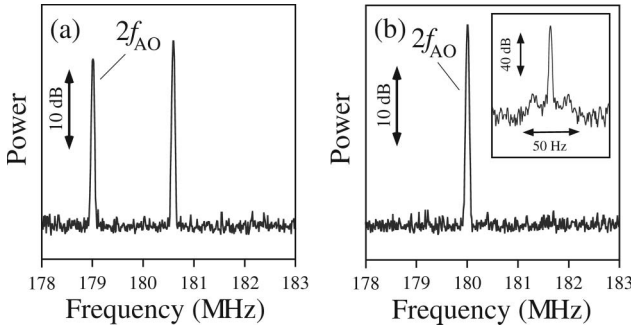

Fig. 3. Typical experimental spectral analysis of the output pulse train power. Resolution bandwidth (RBW) = 30 kHz. (a) Unlocked beat note, i.e., $\Delta\nu > \gamma_e/2\pi$. (b) Locked beat note, i.e., $\Delta\nu < \gamma_e/2\pi$. Inset, RBW = 1 Hz.

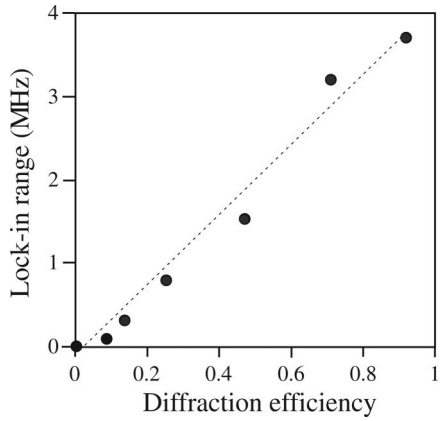

Fig. 4. Experimental cw locking range as a function of the diffraction efficiency of the AO.

In order to check the validity of the model in the PQS case, we integrate Eqs. (4) and (9)–(11) with, in addition to the values given above, the following laser and absorber parameters obtained from [13] and related references: $\gamma_{//} = 4.35 \times 10^3\,\mathrm{s}^{-1}$, $\beta = 0.21$, $T_a = 0.9$, $C_a = 0.03$, $\mu_0 = 2.875$, and $\gamma_a = 2.50 \times 10^5\,\mathrm{s}^{-1}$. This leads to $a_0 = 4.21 \times 10^8\,\mathrm{s}^{-1}$ and $n_0 = 3.85 \times 10^8\,\mathrm{s}^{-1}$. η is equal to 3. The feedback parameters defined by our setup are $\tau = 5\,\mathrm{ns}$, $\Delta\nu = 0$, and $R_3 = 0.4$. Finally, ε was set to 10^{-20}, and the best fit was obtained with $g = 0.3$. The resulting intensity $|E_{\mathrm{out}}|^2$ is plotted in Fig. 5(b) on a single-pulse time window. The agreement with the experimental pulse of Fig. 5(a) is remarkable and validates the model. Besides, we verify that the simulated pulse repetition rate f_{rep} agrees with the experimental one. The approximations used in the delayed differential equations are justified experimentally here because the round-trip time of the laser cavity $2L/c = 0.5\,\mathrm{ns}$ is small compared to the feedback cavity time $\tau = 5\,\mathrm{ns}$, which is itself small compared to the pulse duration of 45 ns.

We now wish to address the question of phase-locking in this PQS regime. It was already proved in [10] that the FSF scheme permits us to induce coherence among successive pulses in the pulse train, i.e., there is also a locking range in the PQS regime. Figure 6 presents the essential experimental features in the electrical spectrum of $|E_{\mathrm{out}}|^2$. First, the beat-note spectrum of the free-running laser appears in Figs. 6(a) and 6(b). In Fig. 6(a), one can see the spectrum centered at 185 MHz, with a FWHM of about 10 MHz. From the analysis of Subsection 2.C, we know that a pulse-to-pulse phase-locked spectrum contains a f_{rep}-periodic frequency comb in this wide envelope. Figure 6(b) hence displays a magnification of the same spectrum, with a frequency span of 100 kHz. From this smooth spectrum, we conclude that the beat-note phase is randomized from pulse to pulse. Second, in the presence of the feedback cavity with a $\Delta\nu$ chosen close to 0, the beat-note spectrum appears in Figs. 6(c) and 6(d). While there is little difference on a frequency span of 80 MHz [see Fig. 6(c) compared to Fig. 6(a)], a magnification on the central frequency at 185 MHz reveals the f_{rep}-periodic frequency comb. From Fig. 2, we conclude that the beat-note phase is locked in the pulse train. We point out that the locking is experimentally robust with respect to acoustic, mechanical, or pump power fluctuations and is independent of the laser excitation rate. We aim to compare these situations, unlocked and locked, with the simulations. We now show that, while experimental locking is straightforwardly observed with the spectrum analyzer, the simulated locking is more easily seen on a temporal basis.

PQS equations are integrated first with a detuning $\Delta\nu = 10\,\mathrm{MHz}$. The resulting output is reported in Fig. 7(a), where both the intensity $|E_{\mathrm{out}}|^2$ and the phase difference $\phi_y - \phi_x$ are displayed. One can see here notably that the phase evolves monotonically with a rate of $2\pi\Delta\nu t$. There is hence no phase locking in this case. When we set $\Delta\nu = 1\,\mathrm{MHz}$, there is a dramatic change in the evolution of $\phi_y - \phi_x$ during the pulse [see Fig. 7(b)]. In this case, there is a clear forcing of the phase difference due to the feedback term. Finally, with a smaller detuning, $\Delta\nu = 100\,\mathrm{kHz}$, the same kind of behavior is observed. From the analysis of many pulses in the train, we find this behavior to be repetitive. Finally, from these simulations, we can estimate a locking range for the PQS case. Indeed, the slope sign change of the phase difference within each pulse gives a relevant indication of phase locking. For the

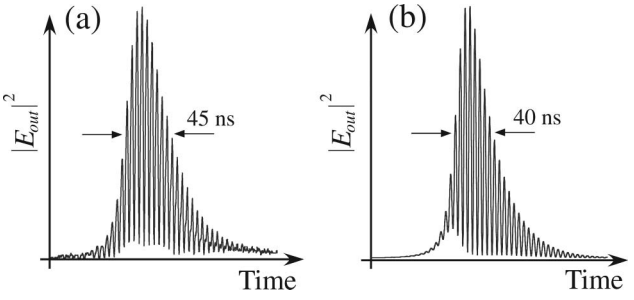

Fig. 5. Output pulse intensity evolution versus time when $f_{\mathrm{rep}} = 10\,\mathrm{kHz}$ and $\Delta\nu = 0$. (a) Experimental pulse. (b) Calculated pulse with the parameters $g = 0.3$, $R_3 = 0.4$, and $\eta = 3$.

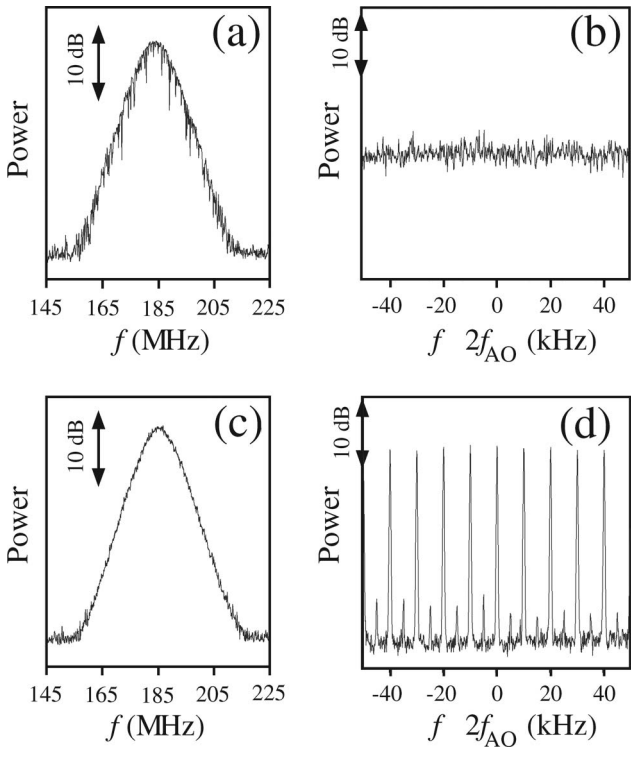

Fig. 6. Experimental spectral analysis of the output power for two different frequency spans. $f_{\mathrm{AO}} = 92.5\,\mathrm{MHz}$. (a), (b) Unlocked regime. (c), (d) Locked regime. (a), (c) RBW = 1 MHz. (b), (d) RBW = 300 Hz.

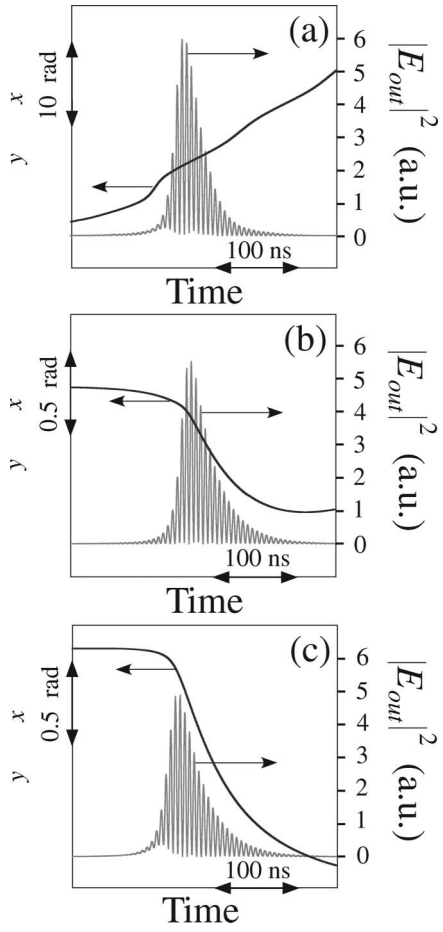

Fig. 7. Calculated intensity and phase difference time evolution for three detunings. (a) $\Delta\nu = 10$ MHz. (b) $\Delta\nu = 1$ MHz. (c) $\Delta\nu = 100$ kHz. The parameters are $g = 1, R_3 = 0.1, \eta = 3$, leading to $\gamma_e/2\pi = 2.2$ MHz.

parameters considered here, it yields a locking range of about 3 MHz ($\gamma_e/2\pi \approx 1.5$ MHz). It is worthwhile to note that a locking range calculated with Eq. (8)—derived in the cw case—yields a value of 4.4 MHz ($\gamma_e/2\pi = 2.2$ MHz). This reduction of the locking range in PQS operation is also observed experimentally: we have observed f_{rep}-periodic combs in the beat-note spectra over a roughly 200 kHz locking range. We suspect the small experimental locking range, compared to the theoretical one, to be due to a weak overlapping factor g or a smaller diffraction efficiency for pulsed feedback. Note that the simulations predict a growing locking range as the feedback strength is increased, and also a quite weak effect of the delay (delays from 1 ns to 10 ns gave similar numerical locking ranges). Finally, we have numerically checked that taking into account multiple delays for the feedback does not change the locking range at the first order.

4. CONCLUSION

We have developed a theoretical model for two-frequency solid-state lasers submitted to a FSF, operating in either the cw or PQS regime. In contrast with previous rate equations models, here the focus is made on the locking of the beat-note frequency with respect to the driving frequency of the AO cell. An experimental setup bearing a dual-polarization diode-pumped Nd:YAG laser and a feedback cavity, containing an AO Bragg cell frequency shifter and a polarization rotator, has been built. In the cw regime, we find an analytical expression for the locking range. The agreement between the theoretical locking range and the experimental one is good. The PQS regime is obtained when a Cr:YAG saturable absorber is inserted inside the laser cavity. Dual-polarized two-frequency pulses are observed, and the effect of FSF is evidenced. Phase locking occurs when the detuning is within a few hundred kilohertz. Here again, a good agreement is found between the simulations and the experimental measures. This pulse-to-pulse coherent regime can find applications, e.g., in lidar-radar systems [18–20]. This study supports previous experimental works on FSF dual-frequency lasers. The model is validated, in particular, with respect to the role of the feedback strength on the locking range. It now permits further investigations on dynamical behaviors linked to the delay [21], in particular, when the detuning is chosen in the vicinity of the relaxation oscillation frequency.

ACKNOWLEDGMENTS

This work was funded in part by the Contrat de Plan Etat-Région "PONANT." We thank T. Erneux and M. Romanelli for fruitful discussions and A. Carré, G. Allio, T. Tressard, and A. Maillocheau for their help.

REFERENCES

1. K. Otsuka and H. Kawaguchi, "Period-doubling bifurcations in detuned lasers with injected signals," Phys. Rev. A **29**, 2953–2956 (1984).
2. K. Otsuka, "Ultrahigh sensitivity laser Doppler velocimetry with a microchip solid-state laser," Appl. Opt. **33**, 1111–1114 (1994).
3. E. Lacot, R. Day, and F. Stoeckel, "Coherent laser detection by frequency-shifted optical feedback," Phys. Rev. A **64**, 043815 (2001).
4. P. Nerin, P. Puget, P. Besesty, and G. Chartier, "Self-mixing using a dual-polarisation Nd:YAG microchip laser," Electron. Lett. **33**, 491–492 (1997).
5. L. Kervevan, H. Gilles, S. Girard, M. Laroche, and P. Leprince, "Self-mixing laser Doppler velocimetry with a dual-polarization Yb:Er glass laser," Appl. Phys. B **86**, 169–176 (2007).
6. F. V. Kowalski, P. D. Hale, and S. J. Shattil, "Broadband continuous-wave laser," Opt. Lett. **13**, 622–624 (1988).
7. H. Guillet de Chatellus and J. P. Pique, "Statistical properties of frequency shifted feedback lasers," Opt. Commun. **283**, 71–77 (2010).
8. H. Sabert and E. Brinkmeyer, "Pulse generation in fiber lasers with frequency shifted feedback," J. Lightwave Technol. **12**, 1360–1368 (1994).
9. L. Kervevan, H. Gilles, S. Girard, and M. Laroche, "Beat-note jitter suppression in a dual-frequency laser using optical feedback," Opt. Lett. **32**, 1099–1101 (2007).
10. M. Brunel and M. Vallet, "Pulse-to-pulse coherent beat note generated by a passively *Q*-switched two-frequency laser," Opt. Lett. **33**, 2524–2526 (2008).
11. R. Lang and K. Kobayashi, "External optical feedback effects on semiconductor injection laser properties," IEEE J. Quantum Electron. **16**, 347–355 (1980).
12. A. E. Siegman, *Lasers* (University Science, 1986).
13. M. Brunel, O. Emile, M. Vallet, F. Bretenaker, A. Le Floch, L. Fulbert, J. Marty, B. Ferrand, and E. Molva, "Experimental and theoretical study of monomode vectorial lasers passively *Q* switched by a Cr^{4+}:yttrium aluminum garnet absorber," Phys. Rev. A **60**, 4052–4058 (1999).
14. A. Le Floch and G. Stephan, "La condition de résonance dans les lasers anisotropes contenant des lames biréfringentes," C. R. Acad. Sci. B **277**, 265–268 (1973).

15. M. Brunel, O. Emile, F. Bretenaker, A. Le Floch, B. Ferrand, and E. Molva, "Tunable two-frequency lasers for lifetime measurements," Opt. Rev. **4**, 550–552 (1997).
16. K. Otsuka, P. Mandel, S. Bielawski, D. Derozier, and P. Glorieux, "Alternate time scale in multimode lasers," Phys. Rev. A **46**, 1692–1695 (1992).
17. N. D. Lai, F. Bretenaker, and M. Brunel, "Coherence of pulsed microwave signals carried by two-frequency solid-state lasers," J. Lightwave Technol. **21**, 3037–3042 (2003).
18. L. J. Mullen, A. J. C. Vieira, P. R. Herczfeld, and V. M. Contarino, "Application of RADAR technology to aerial LIDAR systems for enhancement of shallow underwater target detection," IEEE Trans. Microwave Theory Tech. **43**, 2370–2377 (1995).
19. L. Morvan, N. D. Lai, D. Dolfi, J.-P. Huignard, M. Brunel, F. Bretenaker, and A. Le Floch, "Building blocks for a two-frequency laser lidar-radar: a preliminary study," Appl. Opt. **41**, 5702–5712 (2002).
20. R. Diaz, S.-C. Chan, and J.-M. Liu, "Lidar detection using a dual-frequency source," Opt. Lett. **31**, 3600–3602 (2006).
21. T. Erneux, *Applied Delay Differential Equations* (Springer, 2009).